Residual stiffness of bonded joints for fibre-reinforced polymer profiles

Agostina Orefice[a], Geminiano Mancusi[a,*], Valentino Paolo Berardi[a], Luciano Feo[a], Giulio Zuccaro[b]

[a] Department of Civil Engineering, University of Salerno, Fisciano, Italy
[b] Department of Structures for Engineering and Architecture, University "Federico II", Naples, Italy

ARTICLE INFO

ABSTRACT

In this paper we present an experimental study on the behaviour of samples concerning double lap joints made of glass fibre-reinforced polymer composite (GFRP). According to a multistep displacement/force control procedure, a data driven approach is performed with the aim of investigating the behaviuor of adhesive joints between GFRP profiles at service conditions focusing on the non-linearity of the interfacial damage as the number of cycles increases. The present analysis has been performed regardless of the consideration of material/geometric non-linearities, which affect, instead, the failure load or the buckling limit. The final results provide a database for sketching a predictive rule to be used for a direct evaluation of the loss of stiffness of the joint.

1. Introduction

Composite profiles made of glass fibers (GFRP) are commonly used for civil engineering structures. Within this context their use still surpass the use of carbon fibre-reinforced profiles (CFRP) due to a minor cost. Thereby GFRP profiles are, at the moment, the standard solution for new innovative civil constructions and large scale applications. For these innovative structures the design of connections requires more caution. This is true expecially for the case of adhesive bonding, which represents a field of investigation still open to both theoretical-numerical and experimental contributions [1–8].

Many factors are relevant on the behaviour of adhesive joints, both at the failure point and at service conditions: the thickness and width of the adherents, the number of lap surfaces and the scarf angle (for scarf lap-joints). A recent study about adhesive bonded joints loaded in traction [9] focuses, in a general manner, on this topic.

Although they are widely used in technical practice, adhesive joints for applications of major importance (large truss covers, large bridge decks, or spatial frames) are generally discouraged by the lack of knowledge about their safety and reliability.

The non accuracy of linear models for capturing the mechnical response is the first aspect to be examined. Infact, although the con-

stitutive behaviour of composite materials is usually formulated within a linear-elastic (orthotropic) field, relevant nonlinear effects may emerge over the pre-failure range of the structural response, due to many factors:

- the coupling between axial, flexural, shear, and warping deformations [10–13];
- the time-dependent (delayed) behaviour of GFRP members under dead loads [14–16];
- the "lumped" damage within the bonding interfaces [17,18].

All previous factors exhibit a complex interplay. As a consequence, "all-inclusive" predicting models are not available and data driven approaches may represent, at least for the initial steps of the study, the best choice.

Within this context the present study aims at investigating the behaviuor of adhesive joints between GFRP adherents at service conditions focusing on the non-linearity of the damage behaviour. The present analysis has been performed regardless of the consideration of material/geometric non-linearities, which affect, instead, the failure load or the buckling limit quite above the service loads.
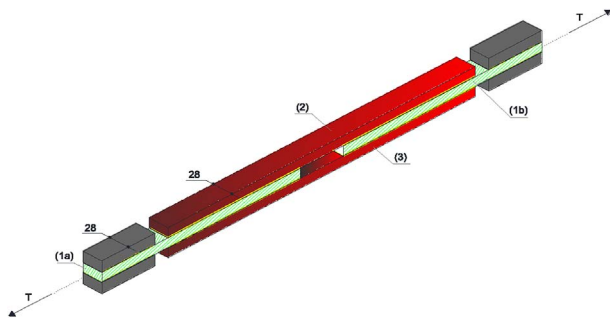

Fig. 1. Joint configuration (axonometric view).

2. Materials and methods

2.1. Experimental design

We propose to investigate the experimental response of composite-to-composite adhesive bonding by a multistep procedure properly designed at the STRENGTH Laboratory of Salerno University (Civil Engineering Department). This approach is discussed in the following with reference to a case study. The sample configuration considered to this scope (a double-lap joint made of GFRP parts), is shown in Figs. 1 and 2 (unit length: mm).

Four adherents can be identified: "1a", "1b", "2", and "3". The cross-section is the same for all of them (28 mm × 14 mm). Each adhesive layer is 1.95 mm thick and is made of an epoxy resin. The mechanical properties of GFRP and adhesive are listed in Tables 1 and 2.

The GFRP adherents were manufactured and provided for free by ATP-Pultrusion S.r.l. (Angri, Italy) as well as the epoxy resin, provided for free by Kerakoll S.p.a (Sassuolo, Italy).

As a preliminary goal, two uniaxial tests have been performed on pure GFRP samples (Figs. 3 and 4) (see Fig. 5).

The setup includes appropriate metal devices for the anchoring into the hydraulic jaws of the testing machine.

Both the preliminary tests (two tests) and the main tests (ten tests) are designed in order to provoke a dominant axial stress state within the joint. A multi-step procedure is followed as indicated in Tables 3 and 4.

In the case of the main tests, strains are monitored by means of 12 uni-axial strain gauges with a grid size of 6.35 mm, characterized by a maximum strain capacity up to 3% and accuracy equal to 10^{-4}% (Fig. 6) (see Fig. 7).

An appropriate protective gel is used in order to ensure the strain gauge reliability. As shown in Fig. 6, strain gauges are applied at

Table 1
Mechanical properties of GFRP (from the manufacturer).

-	Value
Young's modulus	E≥ 30000 N/mm^2
Thermal expansion coefficient	$\alpha \leq 100 \times 10^{-6} \, K^{-1}$
Tensile strength	$f_u \geq 700 \, N/mm^2$
Ultimate tensile strain	$\varepsilon_u \geq 1.50$ %

Table 2
Mechanical properties of Kerabuild Eco Epobond (from the manufacturer).

-	Value	Comments
Young's modulus	$E \geq 2000 \, N/mm^2$	–
Thermal expansion coefficient	$\alpha \leq 100 \times 10^{-6} \, K^{-1}$	$(-25 \, °C \leq T \leq +60 \, °C)$
Bond strength	$\geq 50 \, N/mm^2$	EN 12188 (angle 50°)
	$\geq 60 \, N/mm^2$	EN 12188 (angle 60°)
	$\geq 70 \, N/mm^2$	EN 12188 (angle 70°)

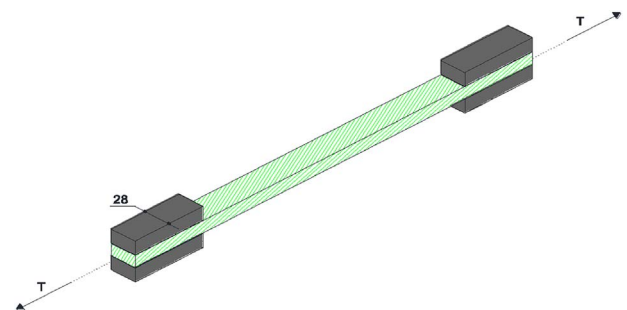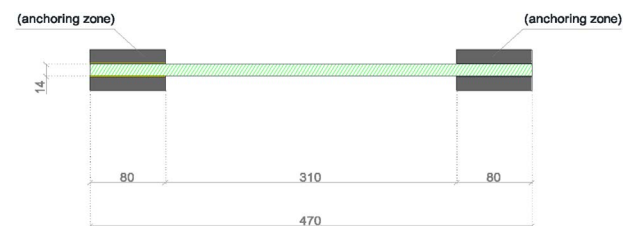**Fig. 3.** Pure GFRP samples (axonometric view).
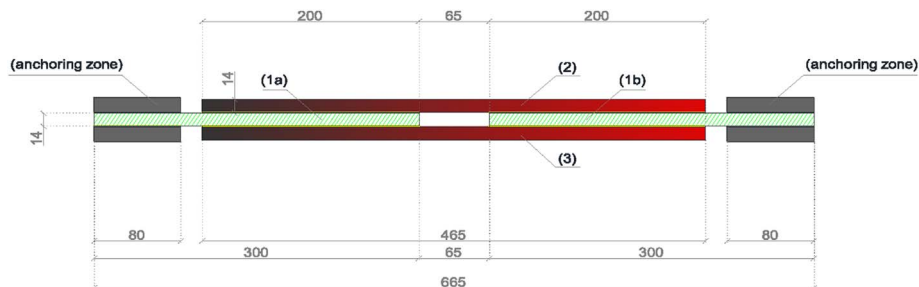

Fig. 4. Pure GFRP samples (side view).

Fig. 2. Joint configuration (side view).

Fig. 5. Preliminary tests on GFRP samples "1" and "2".

Table 3
Multi-step testing procedure (preliminary tests).

Cycles	–		(*)	Target	
1, 2, 3	(a)	loading	DC	+0.50	mm
	(b)	unloading	FC	0.00	N
	(c)	loading	DC	−0.50	mm
	(d)	unloading	FC	0.00	N
4, 5, 6	(a)	loading	DC	+1.00	mm
	(b)	unloading	FC	0.00	N
	(c)	loading	DC	−1.00	mm
	(d)	unloading	FC	0.00	N

(*) DC: displacement control; FC: force control.

Table 4
Multi-step testing procedure (main experiments).

Cycles			(*)	Target	
1, 2, 3	(a)	loading	DC	+1.00	mm
	(b)	unloading	FC	0.00	N
	(c)	loading	DC	0.00	mm
	(d)	unloading	FC	0.00	N
Final		loading (**)	DC	+∞	mm

(*) DC: displacement control; FC: force control; (**) up to failure.

defined positions lying on the external sides of adherents "2" and "3". Four linear variable displacement transducers (LVDTs) are used to measure the global elongation of the joint. The experimental data are acquired by means of a hardware/software system consisting of a data scanner connected to a personal computer. The scanner guarantees an automatic and modulated data acquisition, as well as a real-time adjustment of the data, due to possible loss of the signal.

At a fixed displacement, the current axial force (T), measured by means of a load cell, depends on the stiffness of the entire system (GFRP, adhesive interfaces).

Both the preliminary tests and the main tests are carried out at constant room temperature (18 °C).

The following aspects are investigated:

2.1.1. Via the preliminary axial tests

- the linearity of the response of pure GFRP samples over cycles and the evaluation of the elastic modulus (to be compared with the nominal value given by the manufacturer).

2.1.2. Via the main tests

- the elastic stiffness of the joint;
- the elastic limit of the joint;
- the interfacial damage stored over cycles;
- the strain evolution within the bonding length;
- the failure load of the joint.

Although the failure load of the joint is not the actual scope of this study, its value is evenly detected by means of an additional final step consisting of a monotone loading process (elongation) up to failure.

The testing equipment is presented in the following Fig. 8.

3. Results

The experimental results concern both the constitutive identification of the basic material (GFRP) and the joint behaviour, which is affected by the interfacial damage.

3.1. Preliminary tests

The experimental results presented in Tables 5 and 6 are shown in a sequential order according to the multi-step procedure summarized in Figs. 9 and 10. It is worth noting that the subscripts "0" and "1" respectively indicate the initial point and the end point of the generic step. The symbol "ε" indicates the axial strain while the symbol "σ" is for the axial stress. The amount of non-reversible deformation at the end of the unloading steps (generic step "b" or "d") is also presented.
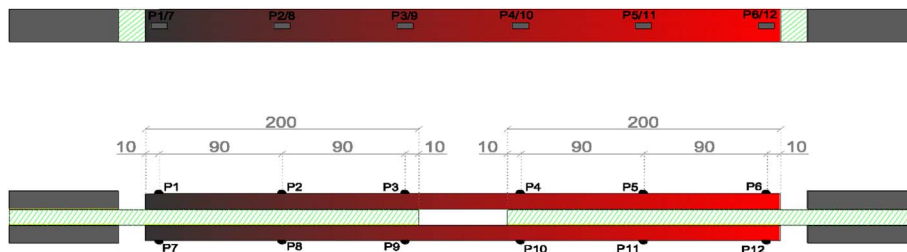

Fig. 6. Strain gauge positions (bottom/top and side view).

Fig. 7. Joint sample "I" (after strain gauges application).

Moreover, the symbol "E_{01}" indicates the Young's modulus evaluated over the generic step by means of a linear fitting of the experimental data.

In Figs. 9 and 10 displacements and axial forces have been converted to non-dimensional quantities with reference to their maximum values, usually attained at the end of the Step 4a.

For sample "1", the value of the Young's modulus (in traction) is equal to 33084 N/mm^2 (average value over cycles 1, 2, and 3) or 30013 N/mm^2 (average value over cycles 4, 5, and 6). The values in compression are, respectively, 37161 N/mm^2 (average value over cycles 1, 2, and 3) and 30994 N/mm^2 (average value over cycles 4, 5, and 6).

For sample "2" the value of the Young's modulus (in traction) is equal to 37093 N/mm^2 (average value over cycles 1, 2, and 3) or 37925 N/mm^2 (average value over cycles 4, 5, and 6) while the values in compression are, respectively, 37023 N/mm^2 (average value over cycles 1, 2, and 3) and 37715 N/mm^2 (average value over cycles 4, 5, and 6).

The previous values represent a better identification of the Young modulus in comparison with the information presented in Table 1. This plays a pivotal role in the evaluation of the mechanical response of the joint sample.

3.2. Main tests

Ten joint samples (J1, …,J10) are tested according to the multistep procedure indicated in Figs. 11–20. The experimental results are presented in Tables 7–16.

Similarly to the case of pure GFRP samples, also for the joint samples the generic step is identified by means of two subscripts, "0" or "1". The symbol "T" is for the axial force while the symbol "ΔL" is for the axial elongation of the joint, evaluated by means of the LVDT signals. It is important to remark that the current elongation of the joint is usually lower than the current target displacement, due to two circumstances: (i) the free elongation of the end of the sample, behind the adhesion zone; and (ii) possible sliding within the anchoring devices.

The amount of non-reversible elongation at the end of the unloading steps is also analyzed. Finally, the symbol "K_{01}" indicates the axial stiffness of the joint, evaluated over the generic step by means of a linear fitting of the experimental data.

Moreover, the experimental failure loads (T_{max}) and the corresponding global elongations (ΔL_{max}) are summarized in Table 17.

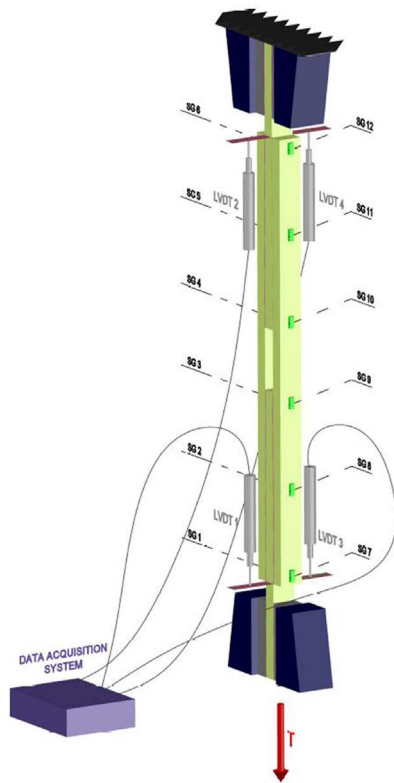The load versus elongation curves are presented in Figs. 21–30.

Fig. 8. Main experiments. Experimental setup.

Table 5
Preliminary tests (GFRP sample "1").

Cycle	Target				ε_o [%]	ε_1 [%]	σ_o [MPa]	σ_1 [MPa]	E_{01} [MPa]
1	loading	1.a	DC	+0.5 mm	0.000	0.161	0.00	53.14	33642
	unloading	1.b	FC	0.0 N	0.161	0.006	53.14	0.00	33349
	loading	1.c	DC	−0.5 mm	0.006	−0.161	0.00	−53.49	32763
	unloading	1.d	FC	0.0 N	−0.161	−0.038	−53.49	0.00	41828
2	loading	2.a	DC	+0.5 mm	−0.038	0.161	0.00	65.62	33221
	unloading	2.b	FC	0.0 N	0.161	−0.030	65.62	0.00	33173
	loading	2.c	DC	−0.5 mm	−0.030	−0.161	0.00	−42.74	32821
	unloading	2.d	FC	0.0 N	−0.161	−0.064	−42.74	0.00	41227
3	loading	3.a	DC	+0.5 mm	−0.064	0.162	0.00	72.79	32515
	unloading	3.b	FC	0.0 N	0.162	−0.055	72.79	0.00	32602
	loading	3.c	DC	−0.5 mm	−0.055	−0.161	0.00	−34.32	32542
	unloading	3.d	FC	0.0 N	−0.161	−0.082	−34.32	0.00	41784
4	loading	4.a	DC	+1.0 mm	−0.082	0.321	0.00	119.45	30426
	unloading	4.b	FC	0.0 N	0.321	−0.006	119.45	0.00	32971
	loading	4.c	DC	−1.0 mm	−0.006	−0.323	0.00	−86.32	27121
	unloading	4.d	FC	0.0 N	−0.323	−0.119	−86.32	0.00	38172
5	loading	5.a	DC	+1.0 mm	−0.119	0.322	0.00	115.97	26826
	unloading	5.b	FC	0.0 N	0.322	−0.005	115.97	0.00	32140
	loading	5.c	DC	−1.0 mm	−0.005	−0.323	0.00	−83.12	26262
	unloading	5.d	FC	0.0 N	−0.323	−0.107	−83.12	0.00	35486
6	loading	6.a	DC	+1.0 mm	−0.107	0.323	0.00	109.51	26016
	unloading	6.b	FC	0.0 N	0.323	0.007	109.51	0.00	31701
	loading	6.c	DC	−1.0 mm	0.007	−0.323	0.00	−82.81	25243
	unloading	6.d	FC	0.0 N	−0.323	−0.098	−82.81	0.00	33678

Table 6
Preliminary tests (GFRP sample "2").

| Cycle	Target				ε_o [%]	ε_1 [%]	σ_o [MPa]	σ_1 [MPa]	E_{01} [MPa]
1	loading	1.a	DC	+0.5 mm	0.000	0.162	0.00	54.44	33986
	unloading	1.b	FC	0.0 N	0.162	0.019	54.44	0.00	36640
	loading	1.c	DC	−0.5 mm	0.019	−0.162	0.00	−62.66	34932
	unloading	1.d	FC	0.0 N	−0.162	−0.004	−62.66	0.00	38586
2	loading	2.a	DC	+0.5 mm	−0.004	0.161	0.00	57.97	35174
	unloading	2.b	FC	0.0 N	0.161	0.021	57.97	0.00	40150
	loading	2.c	DC	−0.5 mm	0.021	−0.162	0.00	−65.81	36181
	unloading	2.d	FC	0.0 N	−0.162	0.008	−65.81	0.00	37717
3	loading	3.a	DC	+0.5 mm	0.008	0.161	0.00	54.91	36079
	unloading	3.b	FC	0.0 N	0.161	0.031	54.91	0.00	40531
	loading	3.c	DC	−0.5 mm	0.031	−0.162	0.00	−70.15	36721
	unloading	3.d	FC	0.0 N	−0.162	0.018	−70.15	0.00	38001
4	loading	4.a	DC	+1.0 mm	0.018	0.323	0.00	107.01	35550
	unloading	4.b	FC	0.0 N	0.323	0.074	107.01	0.00	41001
	loading	4.c	DC	−1.0 mm	0.074	−0.328	0.00	−136.69	34713
	unloading	4.d	FC	0.0 N	−0.328	−0.006	−136.69	0.00	40143
5	loading	5.a	DC	+1.0 mm	−0.006	0.323	0.00	112.47	34268
	unloading	5.b	FC	0.0 N	0.323	0.069	112.47	0.00	40975
	loading	5.c	DC	−1.0 mm	0.069	−0.323	0.00	−137.65	35248
	unloading	5.d	FC	0.0 N	−0.323	−0.007	−137.65	0.00	40376
6	loading	6.a	DC	+1.0 mm	−0.007	0.323	0.00	112.98	34334
	unloading	6.b	FC	0.0 N	0.323	0.069	112.98	0.00	41424
	loading	6.c	DC	−1.0 mm	0.069	−0.323	0.00	−138.01	35554
	unloading	6.d	FC	0.0 N	−0.323	−0.013	−138.01	0.00	40253
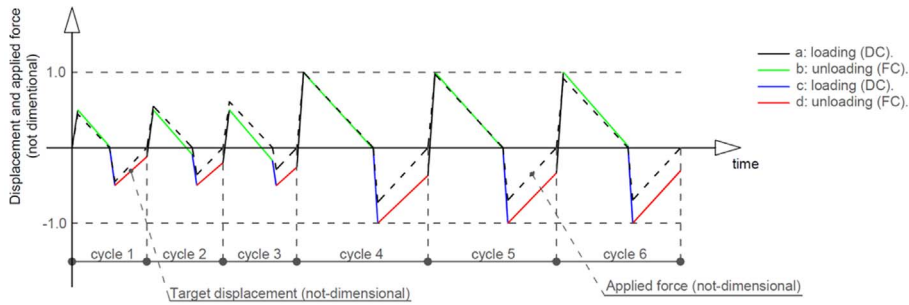
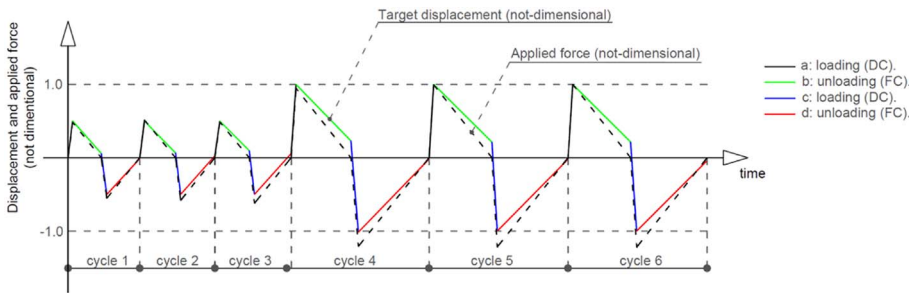**Fig. 9.** Multistep experimental procedure for preliminary tests (GFRP sample "1").

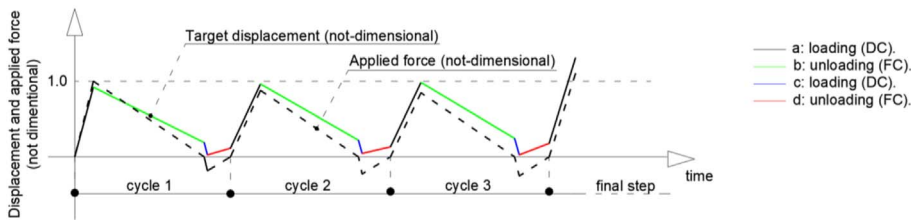**Fig. 10.** Multistep experimental procedure for preliminary tests (GFRP sample "2").

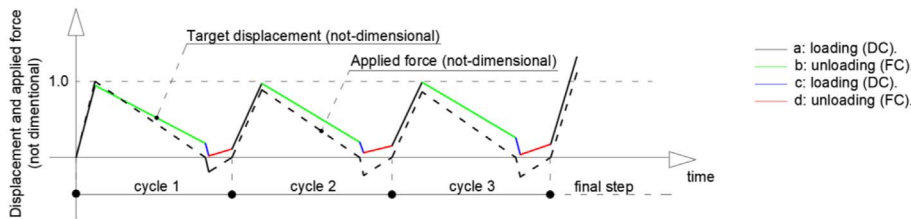**Fig. 11.** Multistep experimental procedure for the joint sample J1.

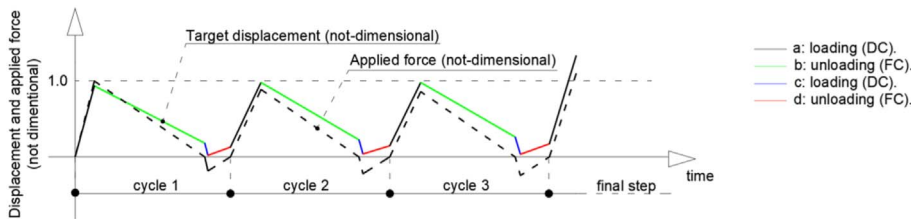**Fig. 12.** Multistep experimental procedure for the joint sample J2.

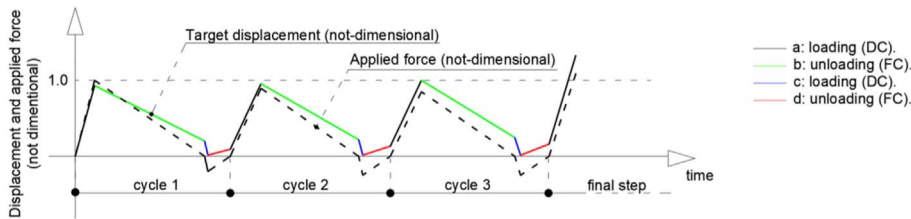**Fig. 13.** Multistep experimental procedure for the joint sample J3.

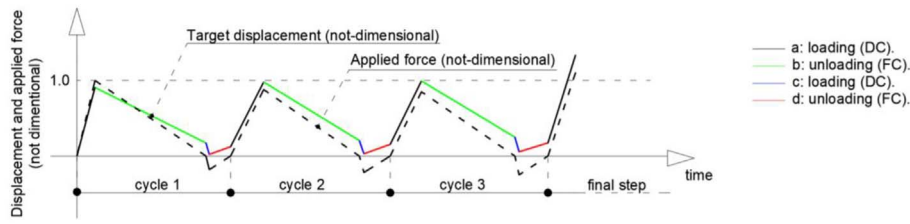**Fig. 14.** Multistep experimental procedure for the joint sample J4.

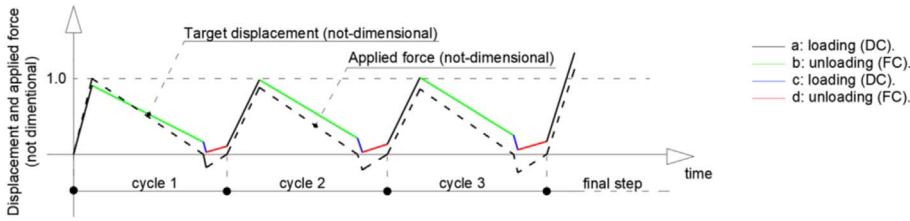Fig. 15. Multistep experimental procedure for the joint sample J5.

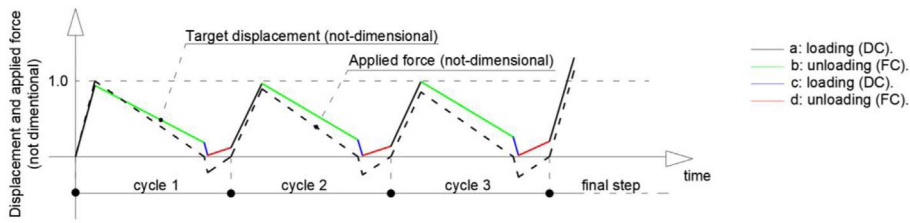Fig. 16. Multistep experimental procedure for the joint sample J6.

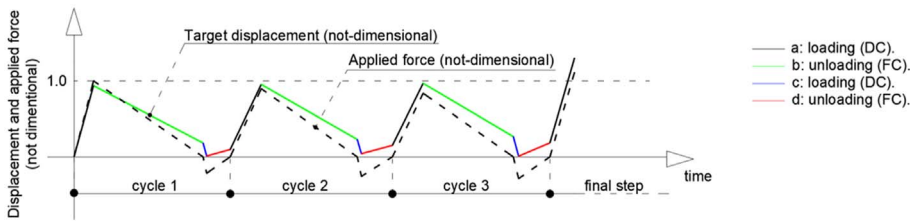Fig. 17. Multistep experimental procedure for the joint sample J7.

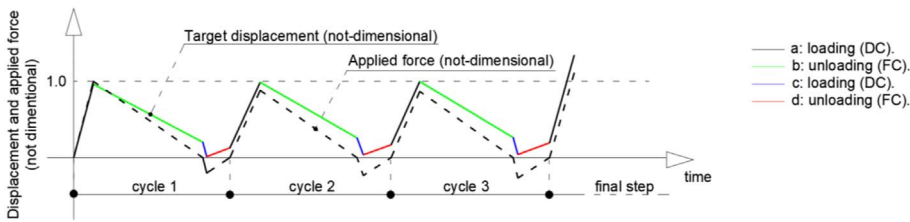Fig. 18. Multistep experimental procedure for the joint sample J8.

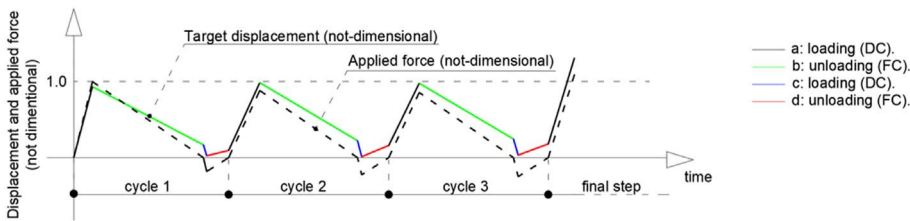Fig. 19. Multistep experimental procedure for the joint sample J9.

Fig. 20. Multistep experimental procedure for the joint sample J10.

Table 7
Main test—joint sample J1.

Cycle	Target				T_o [kN]	T_1 [kN]	ΔL_o [mm]	ΔL_1 [mm]	K_{01} [kN/mm]
1	loading	1.a	DC	+1.0 mm	0.000	40.552	0.0000	0.9208	50459
	unloading	1.b	FC	0.0 N	40.552	0.000	0.9208	0.1889	47474
	loading	1.c	DC	0.0 mm	0.000	−7.465	0.1889	0.0255	48938
	unloading	1.d	FC	0.0 N	−7.465	0.000	0.0255	0.1152	65214
2	loading	2.a	DC	+1.0 mm	0.000	35.588	0.1152	0.9628	44066
	unloading	2.b	FC	0.0 N	35.588	0.000	0.9628	0.2203	44359
	loading	2.c	DC	0.0 mm	0.000	−9.139	0.2203	0.0451	49520
	unloading	2.d	FC	0.0 N	−9.139	0.000	0.0451	0.1331	66079
3	loading	3.a	DC	+1.0 mm	0.000	34.347	0.1331	0.9832	43610
	unloading	3.b	FC	0.0 N	34.347	0.000	0.9832	0.2438	43787
	loading	3.c	DC	0.0 mm	0.000	−10.198	0.2438	0.0267	48033
	unloading	3.d	FC	0.0 N	−10.198	0.000	0.0267	0.1788	60666
	loading	final	DC	→ +∞ mm	0.000	44.700	0.1788	1.3092	44155

Table 8
Main test—joint sample J2.

Cycle	Target				T_o [kN]	T_1 [kN]	ΔL_o [mm]	ΔL_1 [mm]	K_{01} [kN/mm]
1	loading	1.a	DC	+1.0 mm	0.000	40.241	0.0000	0.9462	44166
	unloading	1.b	FC	0.0 N	40.241	0.000	0.9462	0.1855	47174
	loading	1.c	DC	0.0 mm	0.000	−7.667	0.1855	0.0202	48648
	unloading	1.d	FC	0.0 N	−7.667	0.000	0.0202	0.1112	63426
2	loading	2.a	DC	+1.0 mm	0.000	35.749	0.1112	0.9733	43950
	unloading	2.b	FC	0.0 N	35.749	0.000	0.9733	0.2024	44307
	loading	2.c	DC	0.0 mm	0.000	−9.464	0.2024	0.0618	49014
	unloading	2.d	FC	0.0 N	−9.464	0.000	0.0618	0.1533	63892
3	loading	3.a	DC	+1.0 mm	0.000	34.682	0.1533	0.9890	43454
	unloading	3.b	FC	0.0 N	34.682	0.000	0.9890	0.2595	43808
	loading	3.c	DC	0.0 mm	0.000	−10.243	0.2595	0.0367	49110
	unloading	3.d	FC	0.0 N	−10.243	0.000	0.0367	0.1744	59896
	loading	final	DC	→ +∞ mm	0.000	44.826	0.1744	1.3228	43935

Table 9
Main test—joint sample J3.

Cycle	Target				T_o [kN]	T_1 [kN]	ΔL_o [mm]	ΔL_1 [mm]	K_{01} [kN/mm]
1	loading	1.a	DC	+1.0 mm	0.000	40.847	0.0000	0.9364	50599
	unloading	1.b	FC	0.0 N	40.847	0.000	0.9364	0.1811	46628
	loading	1.c	DC	0.0 mm	0.000	−7.542	0.1811	0.0214	46883
	unloading	1.d	FC	0.0 N	−7.542	0.000	0.0214	0.1290	62156
2	loading	2.a	DC	+1.0 mm	0.000	36.299	0.1290	0.9810	44027
	unloading	2.b	FC	0.0 N	36.299	0.000	0.9810	0.2256	44268
	loading	2.c	DC	0.0 mm	0.000	−9.071	0.2256	0.0393	48550
	unloading	2.d	FC	0.0 N	−9.071	0.000	0.0393	0.1472	63113
3	loading	3.a	DC	+1.0 mm	0.000	35.120	0.1472	0.9805	43274
	unloading	3.b	FC	0.0 N	35.120	0.000	0.9805	0.2634	43911
	loading	3.c	DC	0.0 mm	0.000	−10.032	0.2634	0.0351	46268
	unloading	3.d	FC	0.0 N	−10.032	0.000	0.0351	0.1733	58584
	loading	final	DC	→ +∞ mm	0.000	44.912	0.1733	1.3351	42774

Table 10
Main test—joint sample J4.

Cycle	Target				T_o [kN]	T_1 [kN]	ΔL_o [mm]	ΔL_1 [mm]	K_{01} [kN/mm]
1	loading	1.a	DC	+1.0 mm	0.000	40.343	0.0000	0.9307	50822
	unloading	1.b	FC	0.0 N	40.343	0.000	0.9307	0.2010	46570
	loading	1.c	DC	0.0 mm	0.000	−8.048	0.2010	0.0151	45112
	unloading	1.d	FC	0.0 N	−8.048	0.000	0.0151	0.0925	56725
2	loading	2.a	DC	+1.0 mm	0.000	36.052	0.0925	0.9548	43778
	unloading	2.b	FC	0.0 N	36.052	0.000	0.9548	0.2188	44151
	loading	2.c	DC	0.0 mm	0.000	−10.056	0.2188	0.0154	50138
	unloading	2.d	FC	0.0 N	−10.056	0.000	0.0154	0.1330	60009
3	loading	3.a	DC	+1.0 mm	0.000	34.251	0.1330	0.9999	42683
	unloading	3.b	FC	0.0 N	34.251	0.000	0.9999	0.2469	43666
	loading	3.c	DC	0.0 mm	0.000	−10.116	0.2469	0.0145	43632
	unloading	3.d	FC	0.0 N	−10.116	0.000	0.0145	0.1607	55278
	loading	final	DC	→ +∞ mm	0.000	43.926	0.1607	1.3305	42642

Table 11
Main test—joint sample J5.

Cycle	Target				T_o [kN]	T_1 [kN]	ΔL_o [mm]	ΔL_1 [mm]	K_{01} [kN/mm]
1	loading	1.a	DC	+1.0 mm	0.000	41.067	0.0000	0.9072	50812
	unloading	1.b	FC	0.0 N	41.067	0.000	0.9072	0.1730	46886
	loading	1.c	DC	0.0 mm	0.000	−7.388	0.1730	0.0218	46131
	unloading	1.d	FC	0.0 N	−7.388	0.000	0.0218	0.1236	60677
2	loading	2.a	DC	+1.0 mm	0.000	36.133	0.1236	0.9798	42883
	unloading	2.b	FC	0.0 N	36.133	0.000	0.9798	0.2050	44021
	loading	2.c	DC	0.0 mm	0.000	−8.919	0.2050	0.0299	47021
	unloading	2.d	FC	0.0 N	−8.919	0.000	0.0299	0.1550	61926
3	loading	3.a	DC	+1.0 mm	0.000	34.944	0.1550	0.9935	42960
	unloading	3.b	FC	0.0 N	34.944	0.000	0.9935	0.2497	43742
	loading	3.c	DC	0.0 mm	0.000	−10.213	0.2497	0.0563	49656
	unloading	3.d	FC	0.0 N	−10.213	0.000	0.0563	0.1749	59759
	loading	final	DC	→ +∞ mm	0.000	45.331	0.1749	1.3366	42819

Table 12
Main test—joint sample J6.

Cycle	Target				T_o [kN]	T_1 [kN]	ΔL_o [mm]	ΔL_1 [mm]	K_{01} [kN/mm]
1	loading	1.a	DC	+1.0 mm	0.000	40.967	0.0000	0.9085	45178
	unloading	1.b	FC	0.0 N	40.967	0.000	0.9085	0.1635	46817
	loading	1.c	DC	0.0 mm	0.000	−7.132	0.1635	0.0284	45761
	unloading	1.d	FC	0.0 N	−7.132	0.000	0.0284	0.1073	62861
2	loading	2.a	DC	+1.0 mm	0.000	36.115	0.1073	0.9831	44243
	unloading	2.b	FC	0.0 N	36.115	0.000	0.9831	0.2133	44292
	loading	2.c	DC	0.0 mm	0.000	−8.351	0.2133	0.0272	44187
	unloading	2.d	FC	0.0 N	−8.351	0.000	0.0272	0.1342	60633
3	loading	3.a	DC	+1.0 mm	0.000	35.261	0.1342	1.0135	42866
	unloading	3.b	FC	0.0 N	35.261	0.000	1.0135	0.2511	43717
	loading	3.c	DC	0.0 mm	0.000	−9.821	0.2511	0.0606	49902
	unloading	3.d	FC	0.0 N	−9.821	0.000	0.0606	0.1707	59332
	loading	final	DC	→ +∞ mm	0.000	45.962	0.1707	1.3374	42846

Table 13
Main test—joint sample J7.

Cycle	Target				T_o [kN]	T_1 [kN]	ΔL_o [mm]	ΔL_1 [mm]	K_{01} [kN/mm]
1	loading	1.a	DC	+1.0 mm	0.000	39.235	0.0000	0.9410	50453
	unloading	1.b	FC	0.0 N	39.235	0.000	0.9410	0.1856	46591
	loading	1.c	DC	0.0 mm	0.000	−8.291	0.1856	0.0180	47955
	unloading	1.d	FC	0.0 N	−8.291	0.000	0.0180	0.1198	63343
2	loading	2.a	DC	+1.0 mm	0.000	35.157	0.1199	0.9675	42772
	unloading	2.b	FC	0.0 N	35.157	0.000	0.9676	0.2215	44136
	loading	2.c	DC	0.0 mm	0.000	−9.452	0.2216	0.0148	46357
	unloading	2.d	FC	0.0 N	−9.452	0.000	0.0149	0.1387	65389
3	loading	3.a	DC	+1.0 mm	0.000	33.503	0.1387	0.9924	42331
	unloading	3.b	FC	0.0 N	33.503	0.000	0.9925	0.2598	43677
	loading	3.c	DC	0.0 mm	0.000	−10.650	0.2599	0.0161	46483
	unloading	3.d	FC	0.0 N	−10.650	0.000	0.0161	0.2036	59799
	loading	final	DC	→ +∞ mm	0.000	44.623	0.2036	1.3080	42578

Table 14
Main test—joint sample J8.

Cycle	Target				T_o [kN]	T_1 [kN]	ΔL_o [mm]	ΔL_1 [mm]	K_{01} [kN/mm]
1	loading	1.a	DC	+1.0 mm	0.000	39.555	0.0000	0.9372	43172
	unloading	1.b	FC	0.0 N	39.555	0.000	0.9372	0.1829	46577
	loading	1.c	DC	0.0 mm	0.000	−8.528	0.1830	0.0114	48051
	unloading	1.d	FC	0.0 N	−8.528	0.000	0.0114	0.0969	63095
2	loading	2.a	DC	+1.0 mm	0.000	35.476	0.0970	0.9532	42705
	unloading	2.b	FC	0.0 N	35.476	0.000	0.9532	0.2293	44101
	loading	2.c	DC	0.0 mm	0.000	−10.088	0.2293	0.0414	50392
	unloading	2.d	FC	0.0 N	−10.088	0.000	0.0415	0.1517	65572
3	loading	3.a	DC	+1.0 mm	0.000	33.106	0.1518	0.9680	41229
	unloading	3.b	FC	0.0 N	33.106	0.000	0.9681	0.2670	43413
	loading	3.c	DC	0.0 mm	0.000	−11.269	0.2670	0.0089	46701
	unloading	3.d	FC	0.0 N	−11.269	0.000	0.0089	0.1845	59450
	loading	final	DC	→ +∞ mm	0.000	43.957	0.1846	1.2990	42495

Table 15
Main test—joint sample J9.

Cycle	Target				T_o [kN]	T_1 [kN]	ΔL_o [mm]	ΔL_1 [mm]	K_{01} [kN/mm]
1	loading	1.a	DC	+1.0 mm	0.000	40.103	0.0000	0.9624	50661
	unloading	1.b	FC	0.0 N	40.103	0.000	0.9624	0.2029	46540
	loading	1.c	DC	0.0 mm	0.000	−8.119	0.2029	0.0128	45953
	unloading	1.d	FC	0.0 N	−8.119	0.000	0.0129	0.1285	59500
2	loading	2.a	DC	+1.0 mm	0.000	35.356	0.1285	0.9878	43181
	unloading	2.b	FC	0.0 N	35.356	0.000	0.9878	0.2598	44165
	loading	2.c	DC	0.0 mm	0.000	−9.413	0.2599	0.0366	42562
	unloading	2.d	FC	0.0 N	−9.413	0.000	0.0367	0.1682	60910
3	loading	3.a	DC	+1.0 mm	0.000	34.814	0.1683	0.9977	42667
	unloading	3.b	FC	0.0 N	34.814	0.000	0.9978	0.2639	43744
	loading	3.c	DC	0.0 mm	0.000	−10.758	0.2640	0.0406	48934
	unloading	3.d	FC	0.0 N	−10.758	0.000	0.0407	0.1951	58405
	loading	final	DC	→ +∞ mm	0.000	44.504	0.1951	1.3428	42609

Table 16
Main test—joint sample J10.

Cycle	Target				T_o [kN]	T_1 [kN]	ΔL_o [mm]	ΔL_1 [mm]	K_{01} [kN/mm]
1	loading	1.a	DC	+1.0 mm	0.000	40.851	0.0000	0.9337	44566
	unloading	1.b	FC	0.0 N	40.851	0.000	0.9338	0.1675	46756
	loading	1.c	DC	0.0 mm	0.000	−7.437	0.1676	0.0241	46379
	unloading	1.d	FC	0.0 N	−7.437	0.000	0.0242	0.0932	63326
2	loading	2.a	DC	+1.0 mm	0.000	36.049	0.0932	0.9864	43751
	unloading	2.b	FC	0.0 N	36.049	0.000	0.9865	0.2224	44299
	loading	2.c	DC	0.0 mm	0.000	−9.202	0.2224	0.0122	47999
	unloading	2.d	FC	0.0 N	−9.202	0.000	0.0122	0.1587	63507
3	loading	3.a	DC	+1.0 mm	0.000	35.000	0.1587	0.9786	43049
	unloading	3.b	FC	0.0 N	35.000	0.000	0.9786	0.2443	43803
	loading	3.c	DC	0.0 mm	0.000	−10.198	0.2444	0.0322	47726
	unloading	3.d	FC	0.0 N	−10.198	0.000	0.0322	0.1790	60100
	loading	Final	DC	→ +∞ mm	0.000	44.491	0.1791	1.3100	42700

Table 17
Failure loads and global elongations.

Sample	T_{max} [kN]	ΔL_{max} [mm]
J1	44.700	1.3092
J2	44.826	1.3228
J3	44.912	1.3351
J4	43.926	1.3306
J5	45.330	1.3366
J6	45.962	1.3374
J7	44.622	1.3081
J8	43.957	1.2990
J9	44.500	1.3429
J10	44.491	1.3100

Moreover, the analysis of the strain gauge signals represents the required verification of the reliability of the experimental tests.

In Tables 18–27, the strain gradients (de_i/dT) attained within the FRP over the four adhesive interfaces are presented, with e_i being the strain returned by the electrical gauge placed at the location P_i (Fig. 31) and T the applied axial force. The strain gradients have been averaged over the loading step "1a" (cycle 1). Moreover, they are magnified by 1×10^6. Four additional positions have been considered (Q_i, i = 3, 4, 9, 10). They represent relevant cross-sections of the equilibrium scheme depicted in Fig. 31. It is important to underline that the strain gradients at these locations are evaluated from a linear extrapolation based on the actual measurements of the neighboring strain gauges. As an example, the strain at Q_3 has been evaluated accounting for the strains attained at P_1, P_2, and P_3. The last column shows the gradient of the axial force attained within the external adherents of the joint (adherents "2" and
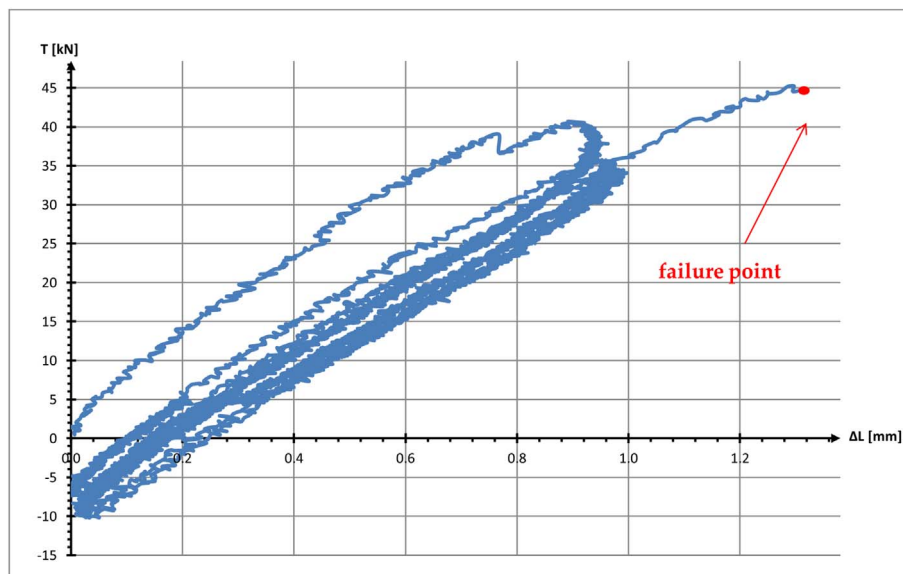

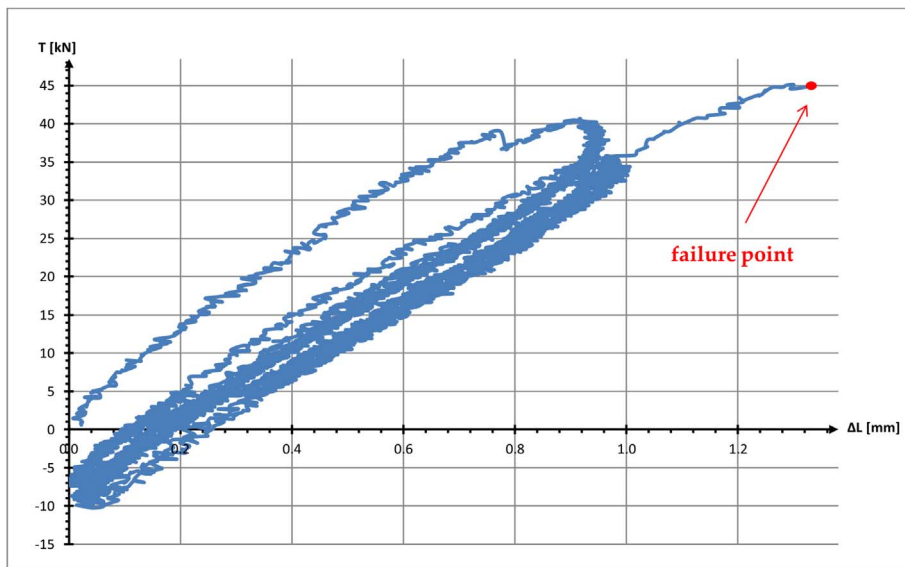**Fig. 21.** Load versus elongation graph—joint sample J1.

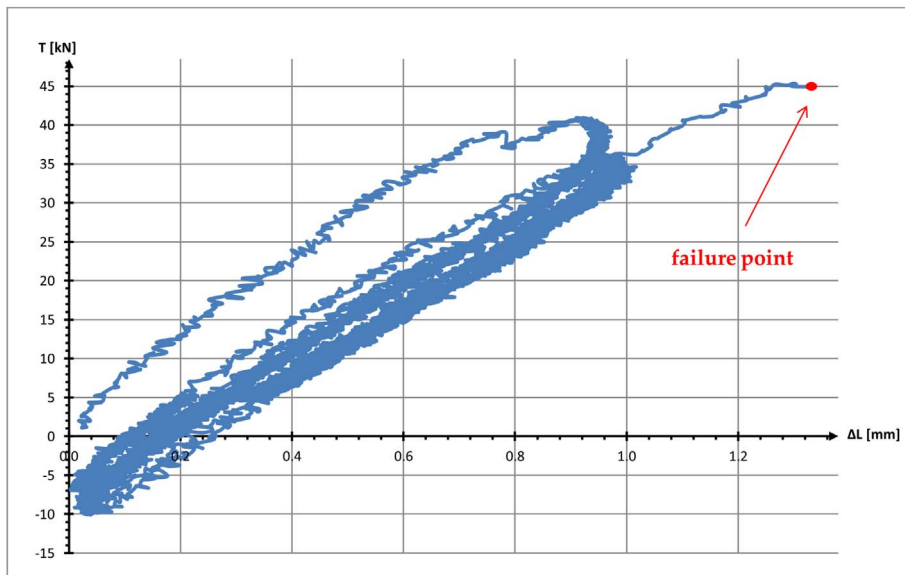**Fig. 22.** Load versus elongation graph—joint sample J2.

Fig. 23. Load versus elongation graph—joint sample J3.

Fig. 24. Load versus elongation graph—joint sample J4.

Fig. 25. Load versus elongation graph—joint sample J5.

Fig. 26. Load versus elongation graph—joint sample J6.
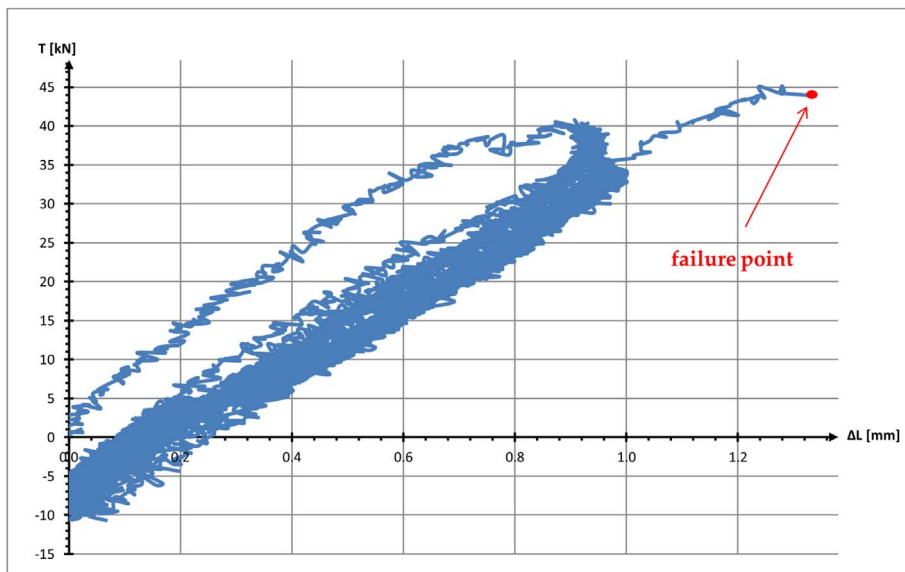

Fig. 27. Load versus elongation graph—joint sample J7.
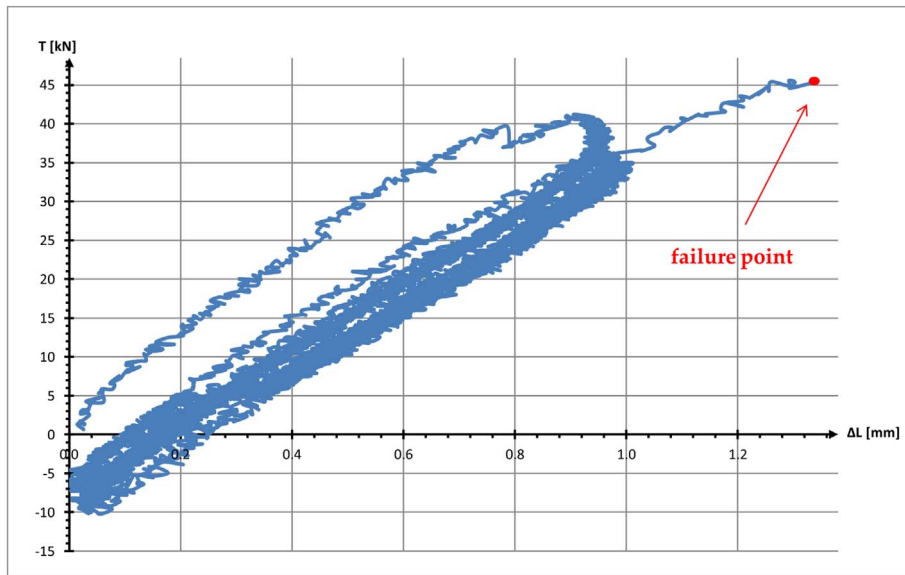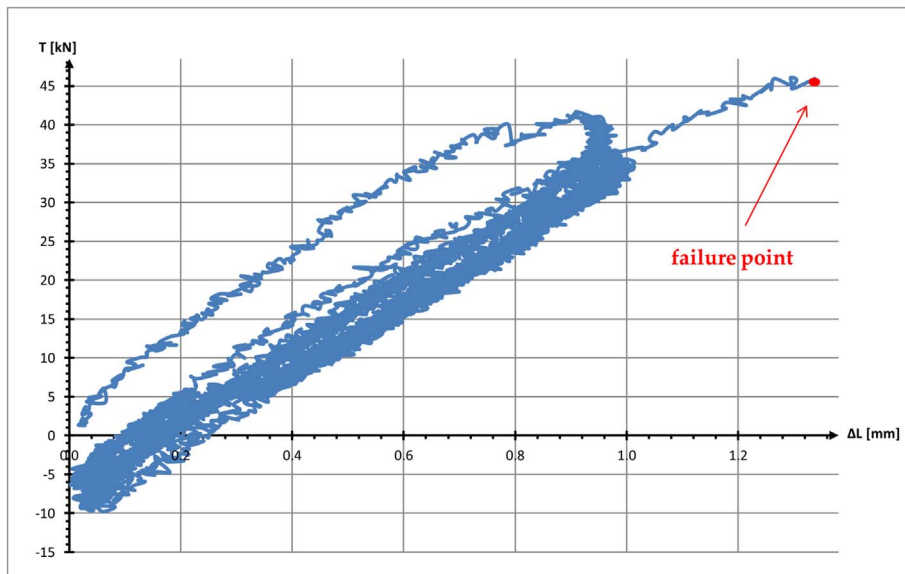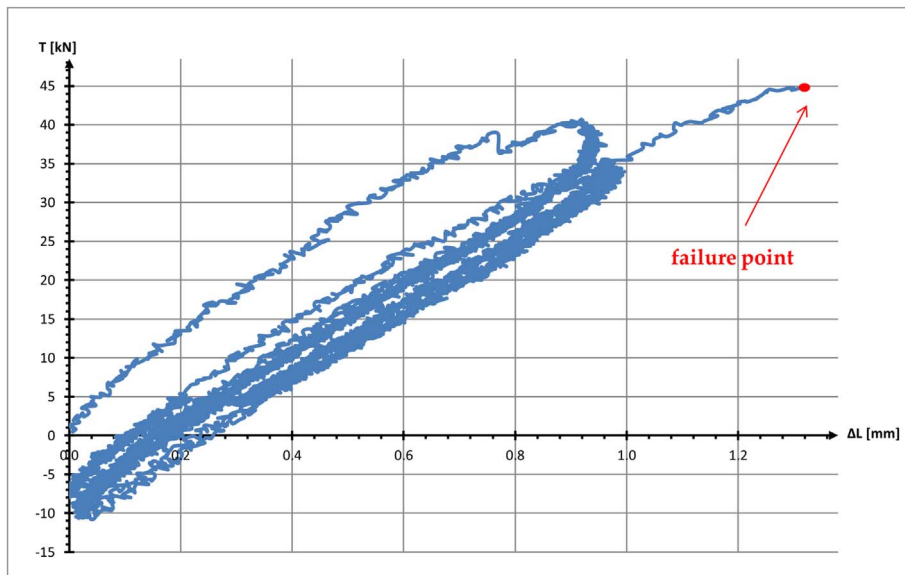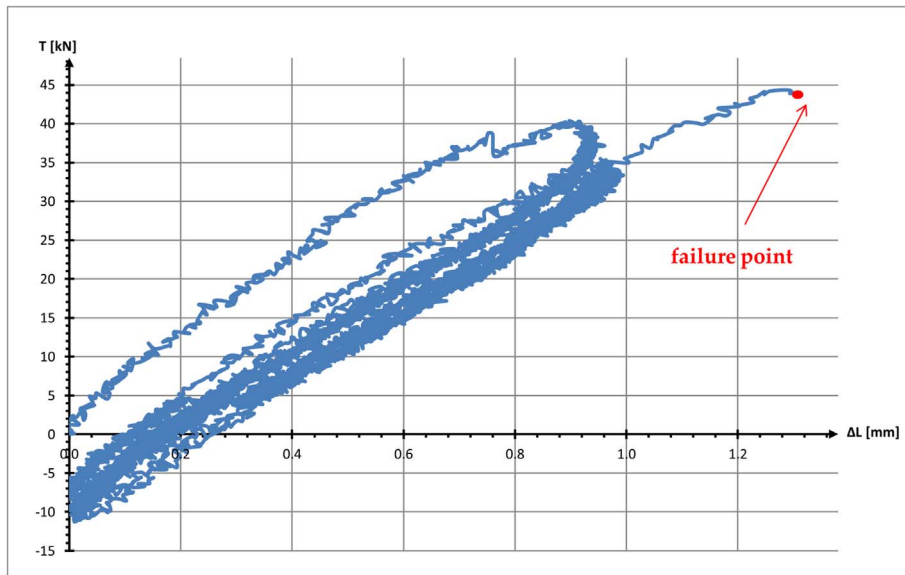
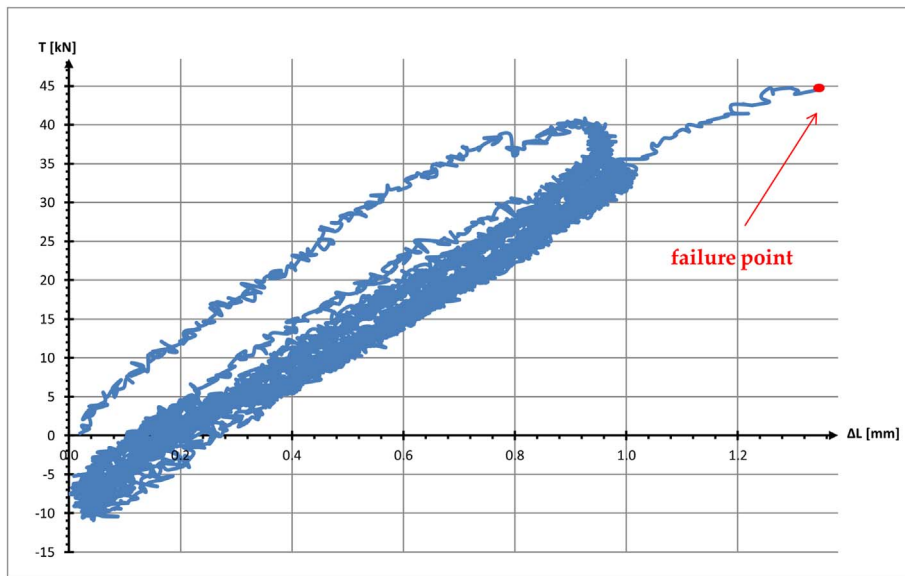**Fig. 28.** Load versus elongation graph—joint sample J8.

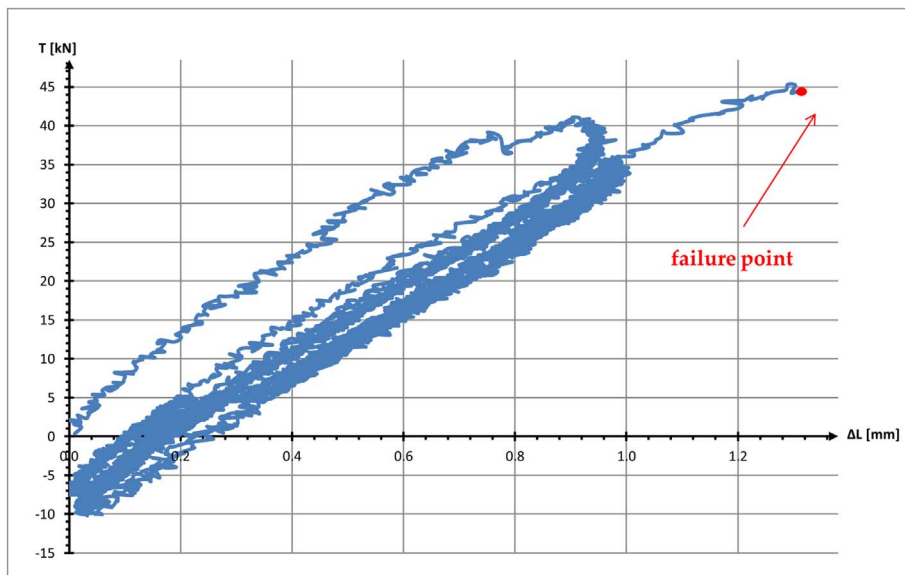**Fig. 29.** Load versus elongation graph—joint sample J9.

Fig. 30. Load versus elongation graph—joint sample J10.

Table 18
Strain and axial force gradients—joint sample J1.

Position	$\frac{de_i}{dT}$ rad $\times 10^6 \times$ N^{-1}	$EA\frac{de_i}{dT}$	Position	$\frac{de_i}{dT}$ rad $\times 10^6 \times$ N^{-1}	$EA\frac{de_i}{dT}$
P_1	0.0082	0.128	P_7	0.0067	0.103
P_2	0.0214	0.332	P_8	0.0150	0.233
P_3	0.0346	0.537	P_9	0.0233	0.362
Q_3	0.0361	0.560	Q_9	0.0242	0.376
Q_4	0.0330	0.513	Q_{10}	0.0271	0.421
P_4	0.0320	0.496	P_{10}	0.0259	0.402
P_5	0.0221	0.343	P_{11}	0.0182	0.283
P_6	0.0123	0.191	P_{12}	0.0038	0.060

Table 22
Strain and axial force gradients—joint sample J5.

Position	$\frac{de_i}{dT}$ rad $\times 10^6 \times$ N^{-1}	$EA\frac{de_i}{dT}$	Position	$\frac{de_i}{dT}$ rad $\times 10^6 \times$ N^{-1}	$EA\frac{de_i}{dT}$
P_1	0.0031	0.049	P_7	0.0027	0.042
P_2	0.0197	0.305	P_8	0.0117	0.181
P_3	0.0362	0.562	P_9	0.0207	0.321
Q_3	0.0380	0.590	Q_9	0.0217	0.336
Q_4	0.0340	0.528	Q_{10}	0.0259	0.402
P_4	0.0325	0.504	P_{10}	0.0247	0.383
P_5	0.0186	0.289	P_{11}	0.0090	0.139
P_6	0.0047	0.073	P_{12}	0.0027	0.043

Table 19
Strain and axial force gradients—joint sample J2.

Position	$\frac{de_i}{dT}$ rad $\times 10^6 \times$ N^{-1}	$EA\frac{de_i}{dT}$	Position	$\frac{de_i}{dT}$ rad $\times 10^6 \times$ N^{-1}	$EA\frac{de_i}{dT}$
P_1	0.0067	0.105	P_7	0.0156	0.243
P_2	0.0204	0.316	P_8	0.0205	0.318
P_3	0.0340	0.528	P_9	0.0254	0.394
Q_3	0.0356	0.552	Q_9	0.0259	0.402
Q_4	0.0328	0.508	Q_{10}	0.0287	0.446
P_4	0.0312	0.483	P_{10}	0.0279	0.433
P_5	0.0168	0.261	P_{11}	0.0192	0.297
P_6	0.0025	0.039	P_{12}	0.0130	0.202

Table 23
Strain and axial force gradients—joint sample J6.

Position	$\frac{de_i}{dT}$ rad $\times 10^6 \times$ N^{-1}	$EA\frac{de_i}{dT}$	Position	$\frac{de_i}{dT}$ rad $\times 10^6 \times$ N^{-1}	$EA\frac{de_i}{dT}$
P_1	0.0087	0.134	P_7	0.0009	0.013
P_2	0.0209	0.324	P_8	0.0129	0.200
P_3	0.0331	0.514	P_9	0.0249	0.386
Q_3	0.0345	0.535	Q_9	0.0262	0.407
Q_4	0.0298	0.462	Q_{10}	0.0313	0.486
P_4	0.0287	0.446	P_{10}	0.0300	0.465
P_5	0.0196	0.304	P_{11}	0.0134	0.207
P_6	0.0105	0.163	P_{12}	0.0052	0.080

Table 20
Strain and axial force gradients—joint sample J3.

Position	$\frac{de_i}{dT}$ rad $\times 10^6 \times$ N^{-1}	$EA\frac{de_i}{dT}$	Position	$\frac{de_i}{dT}$ rad $\times 10^6 \times$ N^{-1}	$EA\frac{de_i}{dT}$
P_1	0.0085	0.131	P_7	0.0011	0.017
P_2	0.0223	0.347	P_8	0.0124	0.193
P_3	0.0362	0.562	P_9	0.0238	0.369
Q_3	0.0378	0.586	Q_9	0.0251	0.389
Q_4	0.0340	0.528	Q_{10}	0.0285	0.442
P_4	0.0326	0.505	P_{10}	0.0273	0.424
P_5	0.0193	0.299	P_{11}	0.0113	0.175
P_6	0.0060	0.093	P_{12}	0.0060	0.093

Table 24
Strain and axial force gradients—joint sample J7.

Position	$\frac{de_i}{dT}$ rad $\times 10^6 \times$ N^{-1}	$EA\frac{de_i}{dT}$	Position	$\frac{de_i}{dT}$ rad $\times 10^6 \times$ N^{-1}	$EA\frac{de_i}{dT}$
P_1	0.0102	0.159	P_7	0.0034	0.052
P_2	0.0224	0.348	P_8	0.0142	0.220
P_3	0.0346	0.537	P_9	0.0250	0.388
Q_3	0.0360	0.558	Q_9	0.0262	0.406
Q_4	0.0347	0.538	Q_{10}	0.0277	0.429
P_4	0.0332	0.515	P_{10}	0.0264	0.409
P_5	0.0201	0.312	P_{11}	0.0114	0.177
P_6	0.0070	0.109	P_{12}	0.0035	0.055

Table 21
Strain and axial force gradients—joint sample J4.

Position	$\frac{de_i}{dT}$ rad $\times 10^6 \times$ N^{-1}	$EA\frac{de_i}{dT}$	Position	$\frac{de_i}{dT}$ rad $\times 10^6 \times$ N^{-1}	$EA\frac{de_i}{dT}$
P_1	0.0078	0.121	P_7	0.0002	0.004
P_2	0.0210	0.325	P_8	0.0133	0.206
P_3	0.0342	0.530	P_9	0.0264	0.409
Q_3	0.0356	0.553	Q_9	0.0278	0.431
Q_4	0.0330	0.512	Q_{10}	0.0301	0.467
P_4	0.0317	0.492	P_{10}	0.0290	0.449
P_5	0.0199	0.309	P_{11}	0.0153	0.238
P_6	0.0081	0.125	P_{12}	0.0081	0.126

Table 25
Strain and axial force gradients—joint sample J8.

Position	$\frac{de_i}{dT}$ rad $\times 10^6 \times$ N^{-1}	$EA\frac{de_i}{dT}$	Position	$\frac{de_i}{dT}$ rad $\times 10^6 \times$ N^{-1}	$EA\frac{de_i}{dT}$
P_1	0.0048	0.074	P_7	0.0017	0.027
P_2	0.0205	0.318	P_8	0.0119	0.185
P_3	0.0362	0.562	P_9	0.0221	0.343
Q_3	0.0380	0.589	Q_9	0.0232	0.360
Q_4	0.0357	0.554	Q_{10}	0.0249	0.387
P_4	0.0340	0.527	P_{10}	0.0238	0.369
P_5	0.0186	0.288	P_{11}	0.0095	0.147
P_6	0.0032	0.050	P_{12}	0.0029	0.044

Table 26
Strain and axial force gradients—joint sample J9.

Position	$\frac{de_i}{dT}$ rad $\times 10^6 \times N^{-1}$	$EA\frac{de_i}{dT}$	Position	$\frac{de_i}{dT}$ rad $\times 10^6 \times N^{-1}$	$EA\frac{de_i}{dT}$
P_1	0.0089	0.138	P_7	0.0082	0.127
P_2	0.0216	0.335	P_8	0.0164	0.255
P_3	0.0342	0.531	P_9	0.0246	0.382
Q_3	0.0356	0.553	Q_9	0.0255	0.396
Q_4	0.0337	0.522	Q_{10}	0.0276	0.428
P_4	0.0322	0.500	P_{10}	0.0264	0.410
P_5	0.0193	0.300	P_{11}	0.0131	0.204
P_6	0.0064	0.100	P_{12}	0.0057	0.089

Table 27
Strain and axial force gradients—joint sample J10.

Position	$\frac{de_i}{dT}$ rad $\times 10^6 \times N^{-1}$	$EA\frac{de_i}{dT}$	Position	$\frac{de_i}{dT}$ rad $\times 10^6 \times N^{-1}$	$EA\frac{de_i}{dT}$
P_1	0.0070	0.109	P_7	0.0037	0.058
P_2	0.0222	0.344	P_8	0.0136	0.211
P_3	0.0374	0.580	P_9	0.0234	0.364
Q_3	0.0390	0.606	Q_9	0.0245	0.381
Q_4	0.0345	0.535	Q_{10}	0.0287	0.445
P_4	0.0331	0.513	P_{10}	0.0273	0.424
P_5	0.0203	0.316	P_{11}	0.0125	0.193
P_6	0.0076	0.118	P_{12}	0.0036	0.055

"3" indicated in Fig. 2). They have been evaluated by means of the following relationship: EA de_i/dT, with EA denoting the axial stiffness of the GFRP adherent (EA = 37000 N/mm^2 × 28 mm × 14 mm), estimated accounting for the experimental characterization of the Young's modulus of the GFRP explained in Section 3.1.

As it is easy to realize, the strain analysis allows the estimation of the gradient of axial forces N′ and N″ with respect to the equilibrium scheme of the joint (Fig. 31). It emerges that the global gradient at the left cross-section Q3–Q9 (dN′/dT + dN″/dT) is substantially equal to
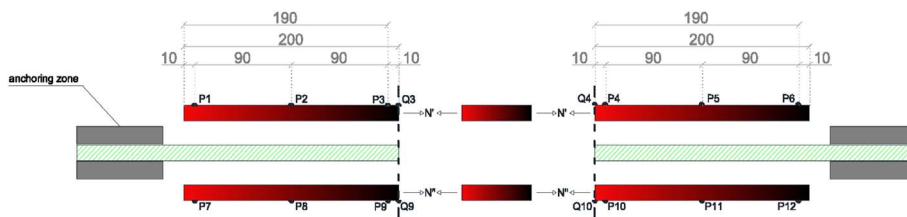
the one attained at the right cross-section Q4–Q10 (dN′/dT + dN″/dT) for all the joint samples, thus indicating that equilibrium is satisfied with a quasi-balanced distribution of the axial forces between the external adherents "2" and "3". It is important to remark that strain gauges are applied to the top/bottom sides of the external adherents and are unable to account for possible shear deformations within the thickness of the GFRP. This in general, together with experimental minor errors, may be responsible for the following apparent paradoxes:

(a) dN′/dT + dN″/dT ≠ 1

(b) dN′/dT|Q₃ ≠ dN′/dT|Q₄

(c) dN″/dT|Q₉ ≠ dN″/dT|Q₁₀

It is worthy of noting that the prediction of the joint behaviour should account for the interfacial damage due to cyclic loads. A possible simple approach may be based on a linear model of the joint where a reduced stiffness is implemented. More in detail, for the above described case study, this can be established considering the average values of the stiffness parameter K_{01} evaluated over the steps 3.a and 3.b, as in Table 28.

The residual stiffness of the joint could be assumed from the average values, provided that an exclusion should occur for data with a difference more than a certain threshold with respect to the stiffness corresponding to the final step. For example, if the chosen threshold is fixed equal to 2%, then all data in Table 28 could be used for calibrating the residual stiffness.

4. Conclusions

In this paper, a study dealing with double lap joints made of GFRP under cyclic loads is conducted. An experimental setup is presented. This is based on a multistep loading/unloading sequence useful to investigate the interfacial damage over cycles. It is shown how the experimental data can be used for estimating, via a simple approach, the residual stiffness of the joint by means of a cautionary reduction of the nominal stiffness value.

Fig. 31. Strain gauges locations and equilibrium scheme (unit length: mm).

Table 28
Stiffness values (K_{01}) – unit: N/mm^2.

Step	J1	J2	J3	J4	J5	J6	J7	J8	J9	J10
3.a (loading)	43610	43454	43274	42683	42960	42866	42331	41229	42667	43049
3.b (unloading)	43787	43808	43911	43666	43742	43717	43677	43413	43744	43803
Average values	43699	43631	43593	43175	43351	43292	43004	42321	43206	43426
Final step values	44155	43935	42774	42642	42819	42846	42578	42495	42609	42700
Diff. [%]	1.04	0.70	1.88	1.23	1.23	1.03	0.99	0.41	1.38	1.67

Acknowledgments

Conflicts of interest

The A.T.P. S.r.l. and Kerakoll S.p.a. companies had no role in this study.

References

[1] Orefice A, Mancusi G, Feo L, Fraternali F. Cohesive interface behaviour and local shear strains in axially loaded composite annular tube. Compos Struct 2017;160:1126–35.

[2] Mancusi G, Orefice A, Feo L, Fraternali F. Structural analysis of adhesive bonding for thick-walled tubular composite profiles. ECCOMAS congress 2016-proceedings of the 7th European congress on computational methods in applied sciences and engineering, vol. 4. 2016. p. 7837–52.

[3] Hasegawa K, Crocombe AD, Coppuck F, Jewell D, Maher S. Characterising bonded joints with a thick and flexible adhesive layer-Part 1: fracture testing and behaviour. Int J Adhes Adhes 2015;63:124–31.

[4] Hasegawa K, Crocombe AD, Coppuck F, Jewell D, Maher S. Characterising bonded joints with a thick and flexible adhesive layer-Part 2: fracture testing and behaviour. Int J Adhes Adhes 2015;63:158–65.

[5] Chaves FJP, Da Silva LFM, De Moura MFSF, Dillard DA, Esteves VHC. Fracture mechanics tests in adhesively bonded joints: a literature review. J Adhes 2014;90:955–92.

[6] Rodríguez RQ, De Paiva WP, Sollero P, Rodrigues MRB, De Albuquerque ÉL. Failure criteria for adhesively bonded joints. Int J Adhes Adhes 2012;37:26–36.

[7] Narayanamurthy V, Chen JF, Cairns J. Improved model for interfacial stresses accounting for the effect of shear deformation in plated beams. Int J Adhes Adhes. 2016;64:33–47.

[8] Mancusi G, Ascione F. Performance at collapse of adhesive bonding. Compos Struct 2013;96:256–61.

[9] Li J, Yan Y, Zhang T, Liang Z. Experimental study of adhesively bonded CFRP joints subjected to tensile loads. Int J Adhes Adhes 2015;57:95–104.

[10] Feo L, Mancusi G. Modeling shear deformability of thin-walled composite beams with open cross-section. Mech Res Commun 2010;37:320–5.

[11] Feo L, Mancusi G. The influence of the shear deformations on the local stress state of pultruded composite profiles. Mech Res Commun 2012;47:44–9.

[12] Mancusi G, Feo L. Non-linear pre-buckling Behaviour of shear deformable thin-walled composite beams with open cross-section. Compos B Eng 2013;47:379–90.

[13] Mancusi G, Ascione F, Lamberti M. Pre-buckling Behaviour of composite beams: a mechanical innovative approach. Compos Struct 2014;117:396–410.

[14] Costa I, Barros J. Tensile creep of a structural epoxy adhesive: experimental and analytical characterization. Int J Adhes Adhes 2015;59:115–24.

[15] Puigvert F, Crocombe AD, Gil L. Fatigue and creep analyses of adhesively bonded anchorages for CFRP tendons. Int J Adhes Adhes. 2014;54:143–54.

[16] Mancusi G, Spadea S, Berardi VP. Experimental analysis on the time-dependent bonding of FRP laminates under sustained loads. Compos B Eng 2013;46:116–22.

[17] Marante ME, Flórez-López J. Three-Dimensional analysis of reinforced concrete frames based on lumped damage mechanics. Int J Solids Struct. 2003;40:5109–23.

[18] Amorim DLDF, Sergio PB, Proença SPB, Flórez-López J. A model of fracture in reinforced concrete arches based on lumped damage mechanics. Int J Solids Struct. 2013;50:4070–9.